Title:

Simultaneous creation of a large vapor plume and pumice raft by a shallow submarine eruption

Authors: Kristen E. Fauria[1*], Martin Jutzeler[2], Tushar Mittal[3], Ashok Gupta[1], Liam J. Kelly[1], John Rausch[1], Ralf Bennartz[1], Brent Delbridge[4], Lise Retailleau[5,6]

Affiliations:

[1]Department of Earth and Environmental Sciences, Vanderbilt University; Nashville, Tennessee, USA

***Corresponding author. Email: kristen.fauria@vanderbilt.edu**

[2]School of Natural Sciences and Centre for Ore Deposit and Earth Sciences (CODES), University of Tasmania, Hobart, Tasmania, Australia

[3]Department of Earth, Atmospheric and Planetary Sciences, Massachusetts Institute of Technology, Cambridge, Massachusetts, USA

[4]EES-17 (Geophysics), Los Alamos National Laboratory, Los Alamos, New Mexico, USA.

[5]Université de Paris, Institut de Physique du Globe de Paris, CNRS, 1 rue Jussieu, F-75005 Paris, France

[6]Observatoire volcanologique du Piton de la Fournaise, Institut de Physique du Globe de Paris, 14 RN3 - Km 27, F-97418 La Plaine des Cafres, La Réunion, France

***Corresponding author. Email: include the email address(es) of the corresponding author(s). Please use the asterisk (*) symbol to denote the corresponding author in the author list and prior to the email address following the affiliations.**

Abstract:

The August 12, 2021 eruption of Fukutoku-Okanoba, a shallow submarine volcano in the Izu-Bonin arc of Japan, is one of few documented submarine eruptions to make a large aerial plume and floating pumice raft. Relative to past eruptions, this event was well-covered by multiple high resolution satellite remote sensors. Here we use satellite remote sensing to assess the eruption style, rates, and products. We find that the 16 km plume was water-rich. Furthermore, we conclude that the 0.1 km^3 raft and 16 km plume were co-genetic and suggest that pumice clasts were delivered to the raft by tephra jets rather than plume fallout. Finally, this eruption highlights a discrepancy between small erupted volumes and high plume heights that may be common for shallow explosive subaqueous eruptions.

One-Sentence Summary: The August 2021 eruption of Fukutoku-Okanoba, Japan is analyzed with multiple high resolution satellite remote sensors.

Main Text:

Submarine volcanoes matter, in part, because they make up the majority of volcanic activity on Earth including a significant fraction of arc volcanism[1]. Submarine volcanic eruptions can also directly impact the atmosphere in cases when they breach the ocean surface. This was clearly illustrated by the January 2022 eruption of Hunga Tonga Hunga Ha'apai, which created damaging ashfall, tsunamis, high atmospheric plumes, and atmospheric shockwaves[2]. Another key aspect of submarine eruptions is that they can create rafts of floating pumice, a highly porous volcanic material that can be hazardous to ships and shore-line infrastructure[3]. For example, the August 2021 Fukutoku-Okanoba pumice raft clogged ports and damaged vessels[4]. Pumice rafts, which can span 100s of km^2, are also important because they transport volcanic material 100s to 1000s of kms over months to years and carry biota[5,6]. Although pumice raft dispersal has been successfully tracked and modeled in a few cases[5,7,8], we lack observations of active pumice raft formation and a basic understanding of how pumice rafts are assembled. Open questions include: *What are the processes that deliver pumice clasts to the sea surface, how do these processes differ compared to those in subaerial settings, and how are rafts related to other eruption features such as aerial plumes?*

Here we report on the August 2021 shallow submarine eruption of Fukutoku-Okanoba, Japan, which created a 16 km water-rich atmospheric plume, 0.1 km^3 raft of floating pumice, and new 1.1 km diameter tuff ring island. We use this eruption as a case study to fill critical gaps in our understanding of raft formation and evolution and therefore constrain conceptual and quantitative models of a key class of submarine eruptions. Specifically, we combine data from more than 12 satellites to assess the eruption stages, styles, rates, and products of this eruption. Excellent observations by the Japan Coast Guard[9] validate and add to parts of this analysis. From the geostationary Himawari-8 data (2 km/pixel resolution, 10 minute frequency), we determine that the eruption sustained a stratospheric, water-ice dominated plume for ~14 hours. Further, we use ultra-high resolution (40 cm/pixel) DigitalGlobe imagery[10] to provide the first observation of the syn-eruptive formation of a large pumice raft. Raft dispersal over the next several days was captured by multiple satellites, providing an exceptional time-series of raft evolution. We observe complex, fine-scale features within the raft and find that the generation and growth of the raft correlates well with the timing of the active aerial plume [Figs. 1 & 2]. Although the raft and plume form concurrently, there is no evidence of clast fallout from the umbrella cloud from satellite imagery and available photos from the Japan Coast Guard. Taken together, our observations suggest that the aerial plume is dominated by water, which stands in stark contrast to stratospheric plumes from subaerial explosive eruptions[11]. We speculate instead, supported by video from the Japan Coast Guard, that pumice clasts are delivered to the raft in high-intensity cock's tail tephra jets[12] that reach to only a few hundreds m high.

By assembling a multi-satellite view of the eruption, we resolve processes such as submarine eruption onset and pumice raft evolution at levels that have not been possible to date. Our study illustrates the importance of high resolution satellite remote sensing datasets to observe and understand volcanic processes at remote volcanoes such as Fukutoku-Okanoba. The implications extend to society, in part, because of the hazards associated with both pumice rafts and aerial eruption columns.

GEOLOGIC BACKGROUND

Fukutoku-Okanoba is an active, shallow submarine arc volcano located 1300 km south of Tokyo in the Bonin Islands where volcanism is associated with subduction of the Pacific Plate beneath the Philippine Sea Plate (Fig. 1B). Over the last century, at least seven eruptions have been documented at Fukutoku-Okanoba, the most recent being in 2010[13]. Confirmed eruptions include those that produced large pumice rafts in 1904, 1914, 1986 and 1992 and temporary islands that were subsequently eroded in 1904, 1914, and 1986[14,15]. All these recent eruptions, and the eruption currently studied, were of intermediate composition (trachyandesite)[14,16,17]. Notably, the 1904 and 1914 eruptions generated weak aerial plumes that, in the case of the 1914 eruption, rose up to 3 km[18,19]. Discolored water activity is also common at the vent site and could indicate continued hydrothermal fluid discharge and/or small eruptions [16]. As recently as 2010, bathymetric surveys showed that Fukutoku-Okanoba was a conical seamount with a 40 mbsl flat oval top (1.7 km x 1.2 km)[20,21].

ERUPTION PROCESSES AND PRODUCTS

The eruption at Fukutoku-Okanoba began on 2021/8/12 21:00 UTC (6:00am 2021/8/13 local time, estimated to the nearest 10 minutes) and was first identified in geostationary Himawari-8 imagery as a bright white aerial plume. During the initial hours of the eruption the plume spread west as an umbrella cloud with an initial volumetric flux of 1.5 x 10^9 m^3 s^{-1} (based on analysis of a spreading gravity current; see Methods; Fig. S1). The plume reached a maximum height of 16 km (a few hundred meters above the mean tropopause height) shortly after eruption onset and remained stratospheric for 14 hours (see Methods and Fig. 1). Over the next 36 hours, the plume became unsteady and waning with multiple smaller pulses. The last pulse visible in Himawari-8 data was at 2021/8/14 23:20 UTC [Fig. 1.], suggesting an end to the main eruption phase. Minor seismicity is observed coincident with the eruption [Figs. S2-S3].

Aerial plume composition:

The composition of the top of the volcanic plume can be assessed using its absorption signature, or more specifically, brightness temperature (BT) and brightness temperature difference (BTD) using Himawari-8. The plume top's brightness temperature was ~200-250 K and its BTD was 0-5 K, indicating the presence of significant ice-particles in the plume [see Methods and Fig. 1]. The World Wide Lightning Location Network reports approximately 10,500 lightning flashes within 40 km of Fukutoku-Okanoba between August 12 and 15[22]. These

flashes are largely coincident with the initial stratospheric plume activity [Fig. 1], which further supports the conclusion that there was significant ice within the plume[23,24]. In addition, ash may have been present in the plume but shielded from satellite sensors because of abundant water and ice, as was the case for the 2016-2017 eruption of Bogoslof, Alaska[25]. Sentinel 5 Tropomi data shows that SO_2 was present in the plume with maximum SO_2 values reaching 10-20 dobson units, DU, less than what was measured in the 2019 eruption of Raikoke Volcano[26,27]. The duration of the SO_2 signature was short (less than four days) compared to eruptions of similar magnitude and at similar latitudes (e.g., the Nishinoshima 2019 eruption, -A.E. Crafford & Venzke, 2020), consistent with the emplacement of water in the stratosphere facilitating the conversion of SO_2 to sulfate aerosols[23].

Relationship between aerial plume and raft formation:

A 7 km diameter pumice raft is visible 4 hours after eruption onset in a Digital Globe ultra-high resolution (0.4 m) image [Fig. 2; 2021/8/13 01:22 UTC]. From this image we see concentric outwards growth of the raft surrounding the white and vapor-rich aerial plume. In the imagery that pre-dates the plume by four hours, there is no clear signature of a pumice raft or discolored water. Given this observation and the highly spatially spread out nature of the raft in the image four hours after plume initiation, we posit that the plume and raft began to form simultaneously, and thus are co-genetic.

We examine all available visual imagery, including Himawari-8, MODIS, and Sentinel-3 data, to evaluate when raft material is present at the vent. Because pumice rafts are quickly transported from their source by ocean currents and wind[7,8], we use the presence of raft material at the vent as an indicator for raft formation. Our ability to resolve the raft's size and location through time is sometimes hindered by: 1) the aerial vapor plume which completely covers the vent area during its most vigorous stage; 2) reduced visual imagery at night; 3) occasional cloud coverage; and 4) the frequency of repeat coverage of medium and high resolution satellites. Despite these challenges, we establish that raft material is at the vent (in all images in which the vent area is visible) during the initial ~60 hours and when large aerial plumes (as defined as being visible in the Himawari-8 data) are created [Fig. 1].

We identify the last large aerial plume pulse from the Himawari-8 data on 2021/8/14 23:20 UTC. However, a video by the Japan Coast Guard on 2021/8/15 4:00 UTC shows an explosion feeding a small vapor plume [9]. Based on this observation, we make a distinction between large, high altitude plumes that are captured by Himawari-8 (2 km/pixel resolution) and small, short-lived and low-altitude plumes that can only be identified in higher resolution satellite imagery or by direct observations. Based on Japan Coast Guard video and satellite imagery that shows raft material near the vent until at least nightfall on August 15 [Fig. 3], we posit that the eruption continued, albeit at a lower intensity, through at least nightfall on August 15 (2021/8/15 8:50 UTC). By following dawn (2021/8/15 20:20 UTC), satellite imagery reveals that the raft had detached from the vent and drifted >12 km north of the vent [movie S2]. Taken

together, our analyses suggest a correlation between eruptive flux into the aerial plume and raft formation. That is, the raft was created while the aerial vapor plume was produced.

New Island:

The exact emergence time of the island remains unknown because the vent area is obstructed by the aerial plume until August 14, when two crescentic islands of 1.1 km diameter are visible [Fig. 3A]. Considering the initial shallow vent depth[20], and the high initial intensity of the eruption, it is highly likely that the island formed during the first day of the eruption itself. We note that the entire eruption was centered within the islands' crater.

Eruption Volume:

We estimate the total raft volume to be ca. 100 mio m^3, based on an average observed area of 250 km^2 and a raft thickness estimate of 40 cm (Jutzeler et al., 2012). Assuming 60% packing of clasts and 70% clast porosities, the total pumice volume is 60 mio m^3 and the dense rock equivalent volume is 18 mio m^3, respectively.

Using the pre-eruption bathymetry, we estimate a submerged sediment volume of ca. 47 mio. m^3, subaerial volume of ca. 6 million m^3, and thus a total minimum new island volume of 53 mio. m^3 (See Methods). The total eruption volume is $O(10^6\ m^3)$ and thus suggests a VEI (volcanic explosivity index) 2 eruption, while the aerial plume height (16 km) indicates a VEI 4 event[29]. The discrepancy is likely a result of the convective nature of the plume and may be typical of submarine eruptions. We consider the event to be VEI 3.

HIGH RESOLUTION ANALYSIS OF THE PUMICE RAFT AND ERUPTION

Four hours after the eruption onset, the first available DigitalGlobe image shows a ~2 km diameter, oval-shaped, feature at sea level with a sharp border that surrounds the vent area [Fig. 2C & 2D]. In part because this feature extends beyond the island, we interpret it to be recently erupted pumice clasts that have been rafted outwards from the vent and into a slightly older and more dilute portion of the raft. We also see water vapor contrails emitted from point sources on the raft that point towards the eruption column [Fig. 2D]. We interpret these to be cooling pumiceous bombs, in part because the steaming intensity decreases outwards from the plume.

All images of the <1-week old pumice raft show bands and complex geometries highlighted by variations in its color [Fig. 3]. We interpret the raft's color and surface morphology to represent differences in raft thickness due to changes in albedo and reflectance properties. Although the specific causes of reflectance changes in rafts have not been studied, thick rafts are achieved through clast stacking[8], which affects surface roughness and likely changes albedo. Thick rafts also raise the top pumice clasts entirely out of seawater[30], where clast drying may contribute to reflectance changes. In the past, evaporation enhanced by the raft has been seen to create low atmospheric clouds above the pumice raft[8].

Figure 3 shows examples of thick and dark portions of the pumice raft grading into thinner and paler areas where ocean swell is observable. The raft's color correlates well with the

amplitude of the local swell [Fig. 3B]. The correlation between color and swell amplitude is repeated throughout the raft images and has also been observed in the 2019 raft from Tonga. Thick rafts are known to dampen swell and waves (Jutzeler et al., 2020) similar to oil slicks (Shen et al., 2019; Zhang et al., 2015) and sea ice[31–33], by reducing wind drag on the ocean surface. We see strong patchwork-like variations in swell dampening that correlate with raft color in the Fukutoku-Okanoba raft [Fig. 3]. Because ca. 30 cm thick pumice rafts have been shown to strongly reduce waves, whereas thin < 10 cm thick rafts have weak to no influence on wave height[8], we interpret the Fukutoku raft to range between 10 and 50 cm in thickness in the first week of dispersal.

The concentric visual patterns present soon after raft formation, interpreted as signatures of thickness differences, are pervasive throughout the following weeks of rafting [Figs. S4-S5]. As the raft moves away from the vent, these patterns have been deformed into complex curves and swirls within the main rafts potentially due to a combination of wind forcing, ocean eddies, and ocean waves. In addition to these swirls, other complex geometries related to collisions between segments of the raft are also common [Fig. 3E]. These structures demonstrate that pumice clasts do not behave as single isolated inertial particles once they are part of a raft but instead have significant particle-particle interaction as in a granular flow. Thus, pumice rafts may provide useful opportunities to test models for the dispersal and transport of sea ice and marine plastics with a different material.

A number of fine-scale structures were present in the raft at proximity to the vent. The proximal raft tracked both radial blast waves that emanated from the vent and ocean swells [Figs. 2 & 3]. The raft interaction with ~NS ocean swells created (~10 m) laminations [Fig. 2B] and and the combined interactions between the raft, radial waves, and ocean swells created interference patterns [Fig. 3D]. Checkerboard patterns were present in the raft in subsequent days [Fig. S4]. We interpret many of these to be due to interaction between wind and ocean waves because the raft fragments were repeatedly oriented parallel to ocean swell and wind directions. None of these small-scale structures are captured by existing raft dispersal models[5,7,8], which describe dynamics at the 10s of km scale. However, these small-scale processes are critical for understanding the initial raft dynamics and for accurate prediction of raft motion near coastal areas where small-scale dynamics control raft motion near harbors or beaches.

We assessed large-scale raft transport velocities for the first week of rafting using imagery from seven satellites [Fig. 2E, Table S1]. During the first weeks of dispersal, the raft traveled 250 km NW at 12–42 km/day (average of 35 km/day), which is faster than the historical worldwide speeds of 6-24 km/day (17 km/day average) (Jutzeler et al., 2014).

In late October 2021, the raft washed up on Okinawa, Japan, ~1400 km west of Fukutoku-Okanoba and later reached the Philippines [34]. The raft caused significant clogging of ports, damage to vessels, and impairment of fishing and tourism industries [35]. Efforts have been underway to remove pumice clasts from ports and track the raft because of its potential impact on Japan's coastal nuclear power plants and harbors[4].

DISCUSSION

Raft generation processes

Despite minimal real-time observations of pumice raft formation to date, a few different processes have been proposed in the literature[36]. Since vapor-filled clasts can be buoyant, it is possible that fragmented clasts can rise buoyantly to the ocean surface[37,38]. Alternatively, raft-forming clasts can be delivered from ballistic ejecta (our current hypothesis), by plume fallout[39], or by pyroclastic currents traveling over water [40] . The satellite and direct visual observations from the initial phase of the Fukutoku-Okanoba eruption provide novel constraints to distinguish among these proposed mechanisms for delivering pumice clasts to the sea surface.

For the Fukutoku-Okanoba eruption, all evidence suggests that the raft was primarily created by ballistic delivery of clasts to the ocean surface by collapsing tephra jets. Satellite imagery shows that the raft was created at or very close to the vent, contrary to a scenario in which a diffuse raft would be created from fallout from a spreading aerial plume (e.g., Elser et al., 2015). A low-resolution video from the Japan Coast Guard on August 13 shows a collapsing jet near the base of a large aerial plume[9]. August 15 Japan Coast Guard video more clearly reveals the ejection of pyroclastic material in classic cocks'tail tephra jets that then fall to the sea surface[41,42]. We therefore posit that tephra jets formed both island and pumice raft [Fig. S6]. Tephra jets may therefore be an important mechanism for pumice raft production in shallow submarine eruptions.

We note, however, that magma-water interactions are known to intensely fragment magma and produce large proportions of <1 mm clasts[43,44]. Pumice rafts, in contrast, are typically made of pumice lapilli and bombs (centimeter to decimeter size clasts [7]). This grain size difference suggests that magma-water interactions may not have been the primary cause of fragmentation.

Particle-plume coupling

The observation that centimeter to decimeter scale pumice raft clasts collapsed from jets and were not carried upwards in the water-rich plume indicates that the rise speed of the plume was slow. Specifically, the rise speed of the plume is required to be less than the fall speed of the clasts[45,46]. Modeling work has shown that external water can suppress the rise speed of plumes within several kms of the vent because of the energy associated with heating and vaporization of water[24,47].

We did not document fine ash within the aerial plume or see evidence for ash fallout (e.g., no discolored water below the aerial plume). Yet, it is possible that small amounts of ash were shielded from satellite sensors and fundamental questions remain regarding the extent to which water-rich plumes are truly tephra poor (especially in fine ash particles). Constraining the nature and amount of fine ash in plumes is critical for assessing aviation and environmental impacts of submarine eruptions. Importantly, unlike ash-rich plumes, vapor-plumes do not create far field deposits and thus are missing from the geological record.

Comparison to other recent subaqueous eruptions

We survey aerial plume heights from other recent submarine eruptions to illustrate the broad importance of understanding the factors that control plume height. Specifically, the 2018 basaltic eruption of Anak Krakatau that created an 18 km ice-rich plume[23,48] and the 2016-2017 trachy-basaltic eruptions of Bogoslof, Alaska generated water-rich aerial plumes that reached up to ~12 km over nine-months[24,25,49]. The January 2022 eruption of Hunga Tonga Hunga Ha'apai created a plume that rose more than 30 km and deposited ash over the Kingdom of Tonga[2]. Going back further in time, the 1984 eruption of Home Reef Volcano, Tonga Islands produced a 0.5 x 1.5 km island, 12 km high plume, and a significant raft of floating pumice [50]. Smaller aerial plumes have been seen such as during the 2012 deep submarine rhyolitic and raft-producing eruption of Havre volcano [7] and from an andesitic eruption at unnamed volcano, Tonga in 2019 which generated a voluminous pumice raft and a small (< 1 km) aerial plume[8]. Previous eruptions at Fukutoku-Okanoba, including ones that formed pumice rafts and a similar sized, if not larger, island had much smaller documented plume heights (max 3 kms). Finally the 1963 basaltic eruption of Surtsey created classic tephra jets and steam-rich eruption columns that rose ~9 km to the tropopause[51]. Like the 2021 Fukutoku-Okanoba eruption[11] note that the 1963 Surtsey eruption displayed, "rapid decoupling and fallout of large poorly fragmented clasts" and that, "the remaining steam-rich parts of the plume rise as a series of thermals." This brief summary illustrates that the features of Fukutoku-Okanoba eruption, including the stratospheric vapor-rich plume, pumice raft, and tephra jetting, are not unique.

The common, yet inconsistent, occurence of vapor-rich aerial plumes leads us to ask why only some shallow subaqueous eruptions produce very high plumes? Unlike dry plumes, vapor-rich plume height may not directly scale with the volume flux of erupted magma[11]. Volcanic Plume models (e.g., plumeria[47]) can help examine how wet plume dynamics change as a function of potential controlling factors such as background atmospheric conditions, the amount of entrained external water, mass flux, vent geometry & depth, and volatile content of the erupted magma. Some modeling results suggest small differences in the initial or boundary conditions of the plume lead to dramatic changes in rise height[23,24,47] and thus determine how submarine eruptions disperse volcanic products and impact processes in the atmosphere.

Summary and future outlook

A clear view of the August 2021 eruption of Fukutoku-Okanoba, Japan was enabled by data from a combination of satellite sensors and complemented by direct observations by the Japan Coast Guard. We determined an initial volume flux of 1.5×10^9 m^3 s^{-1} in the aerial plume using geostationary satellite Himawari-8 data, measured a maximum plume height of 16 km, and documented that the aerial plume contained SO_2 and abundant ice. Central to questions about timing and style of raft creation, we concluded that the 0.1 km^3 raft and stratospheric aerial plume formed simultaneously. However, satellite observations of a water-rich aerial plume and video from the Japan Coast Guard showing tephra jets, together demonstrate that the pyroclasts

were largely decoupled from the aerial plume. Further, we used ultra-high resolution imagery to observe complex structures within the pumice raft, variation in raft thickness, and effects of wind and waves on raft dispersal. We highlight that the total eruption volume, $O(10^6\ m^3)$, and plume height suggest different VEIs.

The August 2021 Fukutoku-Okanoba eruption is unique, in part, because a combination of satellites facilitated integrated analysis to a degree that is largely unprecedented for submarine eruptions [Fig. 4]. Eruption processes that evolve within hours and that are at approximately the meter scale are still not resolvable with current satellite data, however are important for understanding eruption produce delivery mechanisms to the ocean and atmosphere [Fig. 4]. Although our study has relied primarily on visual satellite imagery, future studies can take advantage of the full multispectral information from the various instruments to get more detailed constraints on plume dynamics and raft composition[52], especially high-resolution SAR datasets (e.g., Sentinel-1, NI-SAR, commercial satellites). Additional high-frequency geostationary satellites, such as GEOS and GOCI, may be useful in future studies of volcanic processes. Furthermore, as new types of satellite data become viable (e.g., water vapor isotopes and satellite video over a range of orientations), the possibilities for model testing and process understanding are further expanded[53]. We note that satellite data can be useful even in the absence of physical samples, as was the case for this study. Challenges exist, however, in that many satellites do not have global coverage, especially over the ocean and our analysis relied on fortuitous imagery. High costs can also prohibit scientific access to ultra-high resolution satellite data[54]. Regardless, novel satellite-based observations such as those presented in this study can serve as the foundation for process-based models of important Earth system processes such as volcanic eruptions. Finally, we suggest that studies of sea surface dispersal of plastics, sea ice, and other materials may benefit from a similar multi-satellite and scale perspective.

The presence of a pre-existing multi-disciplinary team of volcano and atmospheric scientists was key to rapidly responding to this event. We highlight this fact in context of current efforts (e.g., CONVERSE) to enable rapid response to volcanic events through US federal support of research networks. The ability to assess satellite remote sensing data is particularly useful in isolated contexts where geophysical monitoring data are limited (e.g. seismicity, GNSS).

Satellite data is well-suited to answer important questions about the nature of submarine volcanism, through study of their eruption columns and pumice rafts, especially when volcanoes are remote or when physical sampling is not possible. Thus, we strongly recommend that medium and ultra-high resolution satellites should be tasked to image known submarine volcanoes to determine background conditions, identify eruptions, and as part of coordinated rapid responses.

REFERENCES

1. Crisp, J. A. Rates of magma emplacement and volcanic output. *J. Volcanol. Geotherm. Res.*

20, 177–211 (1984).

2. Global Volcanism Program. *Report on Hunga Tonga-Hunga Ha'apai (Tonga)*. (2022).
3. Risso, C., Scasso, R. A. & Aparicio, A. Presence of large pumice blocks on Tierra del Fuego and South Shetland Islands shorelines, from 1962 South Sandwich Islands eruption. *Mar. Geol.* **186**, 413–422 (2002).
4. Yamaguchi, M. Pumice pileup from undersea volcano causing damage in Japan. *Associated Press* (2021).
5. Bryan, S. E. *et al.* Pumice rafting and faunal dispersion during 2001–2002 in the Southwest Pacific: record of a dacitic submarine explosive eruption from Tonga. *Earth Planet. Sci. Lett.* **227**, 135–154 (2004).
6. Freundt, A., Schindlbeck-Belo, J. C., Kutterolf, S. & Hopkins, J. L. Tephra layers in the marine environment: A review of properties and emplacement processes. *Geol. Soc. Lond. Spec. Publ.* **520**, (2021).
7. Jutzeler, M. *et al.* On the fate of pumice rafts formed during the 2012 Havre submarine eruption. *Nat. Commun.* **5**, 3660 (2014).
8. Jutzeler, M. *et al.* Ongoing Dispersal of the 7 August 2019 Pumice Raft From the Tonga Arc in the Southwestern Pacific Ocean. *Geophys. Res. Lett.* **47**, e1701121 (2020).
9. Submarine volcano database. *Fukutoku Okanoba* https://www1.kaiho.mlit.go.jp/GIJUTSUKOKUSAI/kaiikiDB/kaiyo24-2.htm (2021).
10. Neigh, C. S. R., Masek, J. G. & Nickeson, J. E. High-Resolution Satellite Data Open for Government Research. *Eos Trans. Am. Geophys. Union* **94**, 121–123 (2013).
11. Carey, S. & Bursik, M. Volcanic Plumes. in *The Encyclopedia of Volcanoes* 571–585 (Elsevier, 2015). doi:10.1016/B978-0-12-385938-9.00032-8.
12. White, J. D. L., Schipper, C. I. & Kano, K. Chapter 31 - Submarine Explosive Eruptions. in *The Encyclopedia of Volcanoes (Second Edition)* (ed. Sigurdsson, H.) 553–569 (Academic Press, 2015). doi:10.1016/B978-0-12-385938-9.00031-6.

13. Smithsonian Institution & Venzke, E. Volcanoes of the World, v. 4.3.4. (2013).
14. Furukawa, H. Annual report of the world volcanic eruptions in 1992. *Bull. Volcan. Erupt.* **57**, 81–82 (1992).
15. Urai, M. Time series analysis of discolored seawater reflectance observed by Advanced Visible and Near Infrared Radiometer type 2 (AVNIR-2) at Fukutoku-Okonaba submarine volcano, Japan. *J. Volcanol. Geotherm. Res.* **269**, 23–27 (2014).
16. Japan Meteorological Agency. *Fukutoku-Okanoba* https://www.data.jma.go.jp/svd/vois/data/tokyo/331_Fukutoku-Oka-no-Ba/331_index.html (2013).
17. Yoshida, K. *et al.* Variety of the drift pumice clasts from the 2021 Fukutoku-Oka-no-Ba eruption, Japan. (2021).
18. Kuno, H. Iwo-Zima (8,4 - 12). in *Catalogue of the active volcanoes of th world, including solfatara fields of Imperial Earthquake Investigation Committee* 259–265 (International Volcanological Association, 1962).
19. Wakimizu, T. The ephemeral volcanic island in the Iwojima Group. *Earthq. Investig. Comm.* **22**, 1–33 (1908).
20. Ito K., Kato S., Takahashi M. & Saito A. Volcanic topography of Fukutoku−Oka-no-ba volcano in Izu-Ogasawara arc after the 2010 eruption. (2011).
21. Otani Y. *et al.* Observation on Fukutoku−Oka−no−Ba submarine volcano eruption in 2005. (2006).
22. Lay, E. H. WWLL global lightning detection system: Regional validation study in Brazil. *Geophys. Res. Lett.* **31**, L03102 (2004).
23. Prata, A. T. *et al.* Anak Krakatau triggers volcanic freezer in the upper troposphere. *Sci. Rep.* **10**, 3584 (2020).
24. Van Eaton, A. R. *et al.* Did ice-charging generate volcanic lightning during the 2016–2017 eruption of Bogoslof volcano, Alaska? *Bull. Volcanol.* **82**, 24 (2020).

25. Schneider, D. J., Van Eaton, A. R. & Wallace, K. L. Satellite observations of the 2016–2017 eruption of Bogoslof volcano: aviation and ash fallout hazard implications from a water-rich eruption. *Bull. Volcanol.* **82**, 29 (2020).
26. de Leeuw, J. *et al.* The 2019 Raikoke volcanic eruption – Part 1: Dispersion model simulations and satellite retrievals of volcanic sulfur dioxide. *Atmospheric Chem. Phys.* **21**, 10851–10879 (2021).
27. McKee, K. *et al.* Evaluating the state-of-the-art in remote volcanic eruption characterization Part I: Raikoke volcano, Kuril Islands. *J. Volcanol. Geotherm. Res.* **419**, 107354 (2021).
28. A.E. Crafford & Venzke, E. Global Volcanism Program. *Report on Nishinoshima (Japan)* https://volcano.si.edu/ShowReport.cfm?doi=10.5479/si.GVP.BGVN202009-284096 (2020).
29. Newhall, C. G. & Self, S. The volcanic explosivity index (VEI) an estimate of explosive magnitude for historical volcanism. *J. Geophys. Res. Oceans* **87**, 1231–1238 (1982).
30. Simkin, T. & Fiske, R. S. Krakatau 1883: A classic geophysical event. *Eos Trans. Am. Geophys. Union* **64**, 513–514 (1983).
31. Kohout, A. L. *et al.* Observations of exponential wave attenuation in Antarctic sea ice during the PIPERS campaign. *Ann. Glaciol.* **61**, 196–209 (2020).
32. Passerotti, G. *et al.* Interactions between irregular wave fields and sea ice: A physical model for wave attenuation and ice break up. *ArXiv211012659 Phys.* (2021).
33. Rogers, W. E., Yu, J. & Wang, D. W. Incorporating dependence on ice thickness in empirical parameterizations of wave dissipation by sea ice. *ArXiv210401246 Phys.* (2021).
34. GDAPD. PRIMER ON THE FLOATING PUMICE STONES & VOLCANIC DEBRIS ON THE SHORES OF BATANES PROVINCE: AFTERMATH OF THE AUGUST 2021 ERUPTION OF FUKUTOKU-OKANOBA SUBMARINE VOLCANO IN JAPAN. https://www.phivolcs.dost.gov.ph/index.php/news/13373-primer-on-the-floating-pumice-stones-volcanic-debris-on-the-shores-of-batanes-province-aftermath-of-the-august-2021-eruption-of-fukutoku-okanoba-submarine-volcano-in-japan.

35. Kyodo News, K. Okinawa starts removing pumice stones after volcanic eruption. *Kyodo News+* https://english.kyodonews.net/news/2021/10/3678b725358d-okinawa-starts-removing-pumice-stones-after-volcanic-eruption.html (2021).
36. Cas, R. A. F. & Giordano, G. Submarine Volcanism: a Review of the Constraints, Processes and Products, and Relevance to the Cabo de Gata Volcanic Succession. *Ital. J. Geosci.* **133**, 362–377 (2014).
37. Allen, S. R. & McPhie, J. Products of neptunian eruptions. *Geology* **37**, 639–642 (2009).
38. Fauria, K. E. & Manga, M. Pyroclast cooling and saturation in water. *J. Volcanol. Geotherm. Res.* **362**, 17–31 (2018).
39. Elser, J. J. *et al.* Community Structure and Biogeochemical Impacts of Microbial Life on Floating Pumice. *Appl. Environ. Microbiol.* **81**, 1542–1549 (2015).
40. Dufek, J., Wexler, J. & Manga, M. Transport capacity of pyroclastic density currents: Experiments and models of substrate-flow interaction: TRANSPORT CAPACITY OF PYROCLASTIC FLOWS. *J. Geophys. Res. Solid Earth* **114**, (2009).
41. Houghton, B., White, J. D. L. & Van Eaton, A. R. Phreatomagmatic and Related Eruption Styles. in *The Encyclopedia of Volcanoes* 537–552 (Elsevier, 2015). doi:10.1016/B978-0-12-385938-9.00030-4.
42. Kokelaar, B. P. The mechanism of Surtseyan volcanism. *J. Geol. Soc.* **140**, 939–944 (1983).
43. Sheridan, M. F. & Wohletz, K. H. Hydrovolcanism: Basic considerations and review. *J. Volcanol. Geotherm. Res.* **17**, 1–29 (1983).
44. Walker, G. P. L. Explosive volcanic eruptions — a new classification scheme. *Geol. Rundsch.* **62**, 431–446 (1973).
45. Carey, S. & Sparks, R. S. J. Quantitative models of the fallout and dispersal of tephra from volcanic eruption columns. *Bull. Volcanol.* **48**, 109–125 (1986).
46. Lippert, M. C. & Woods, A. W. Particle fountains in a confined environment. *J. Fluid Mech.* **855**, 28–42 (2018).

47. Mastin, L. G. A user-friendly one-dimensional model for wet volcanic plumes. *Geochem. Geophys. Geosystems* **8**, (2007).
48. Fiantis, D. *et al.* Geochemical and mineralogical composition of the 2018 volcanic deposits of Mt. Anak Krakatau. *Geoderma Reg.* **25**, e00393 (2021).
49. Coombs, M. *et al.* Overview, chronology, and impacts of the 2016–2017 eruption of Bogoslof volcano, Alaska. *Bull. Volcanol.* **81**, 62 (2019).
50. McClelland, L. *Global Volcanism Program*. https://doi.org/10.5479/si.GVP.SEAN198404-243080 (1984).
51. Thorarinsson, S., Einarsson, Th., Sigvaldason, G. & Elisson, G. The submarine eruption off the Vestmann islands 1963–64: A preliminary report. *Bull. Volcanol.* **27**, 435–445 (1964).
52. Williams, D. B. & Ramsey, M. S. Analysis of ash emissions from the 2020 Nishinoshima eruption using ASTER thermal infrared orbital data. *J. Volcanol. Geotherm. Res.* **421**, 107424 (2022).
53. Tada, M., Yoshimura, K. & Toride, K. Improving weather forecasting by assimilation of water vapor isotopes. *Sci. Rep.* **11**, 18067 (2021).
54. Kraetzig, N. M. A Definitive Guide to Buying and Using Satellite Imagery. *UP42 Official Website* https://up42.com/blog/tech/a-definitive-guide-to-buying-and-using-satellite-imagery (2021).
55. Planet Team. *Planet Application Program Interface: In Space for Life on Earth*. (Planet Labs, 2017).
56. Hersbach, H. *et al.* The ERA5 global reanalysis. *Q. J. R. Meteorol. Soc.* **146**, 1999–2049 (2020).
57. Atkinson, J. Enhanced Stratospheric Aerosols from Fukutoku-Okanoba Eruption. *NASA* http://www.nasa.gov/feature/langley/enhanced-stratospheric-aerosols-from-fukutoku-okanoba-eruption (2021).
58. World Metorological Organization. Definition of the tropopause. *WMO Bull* **6**, 136 (1957).

59. Simurda, C., Magruder, L. A., Markel, J., Garvin, J. B. & Slayback, D. A. ICESat-2 Applications for Investigating Emerging Volcanoes. *Geosciences* **12**, 40 (2022).

60. Winker, D. M., Hunt, W. H. & McGill, M. J. Initial performance assessment of CALIOP. *Geophys. Res. Lett.* **34**, (2007).

Acknowledgments:
DigitalGlobe/Maxar data were provided by the Commercial Archive Data for NASA investigators (cad4nasa.gsfc.nasa.gov) under the National Geospatial-Intelligence Agency's NextView license agreement. We thank the Massachusetts Institute of Technology Library for providing access to imagery from Planet Labs. The *Himawari-8* radiance data are obtained from the National Institute of Information and Communications Technology (NICT) Science Cloud, Japan. The authors wish to thank the World Wide Lightning Location Network (http://wwlln.net), a collaboration among over 50 universities and institutions, for providing the lightning location data used in this paper. The local earthquakes location was extracted from the USGS earthquakes catalog (earthquake.usgs.gov/earthquakes). The seismic recordings were accessed through the IRIS datacenter (http://www.iris.edu/mda) with the module Obspy. We thank Michael Manga for reviewing an earlier version of this manuscript.

Funding: This work was funded by National Aeronautics and Space Administration grant 80NSSC20K1450 (K.E.F., R.B., A.G., L.K.). TM was supported by a Massachusetts Institute of Technology Crosby fellowship.

Author contributions:

Conceptualization: KEF, MJ, TM

Methodology: AG, MJ, TM, KEF, RB, JR, BD, LR

Investigation: AG, MJ, TM, KEF, LK, JR, BD, LR

Visualization: KEF, MJ, TM, AG, LK, LR

Funding acquisition: KEF, RB

Project administration: KEF, MJ, TM

Supervision: KEF, TM, RB

Writing – original draft: KEF, AG, MJ, TM

Writing – review & editing: RB, LR, BD, LK

Competing interests: Authors declare that they have no competing interests.

Data and materials availability: Code and materials used in this analysis will be made available in a public database. This database will provide instructions on how to access the publicly available satellite data used in this study.

Figures:

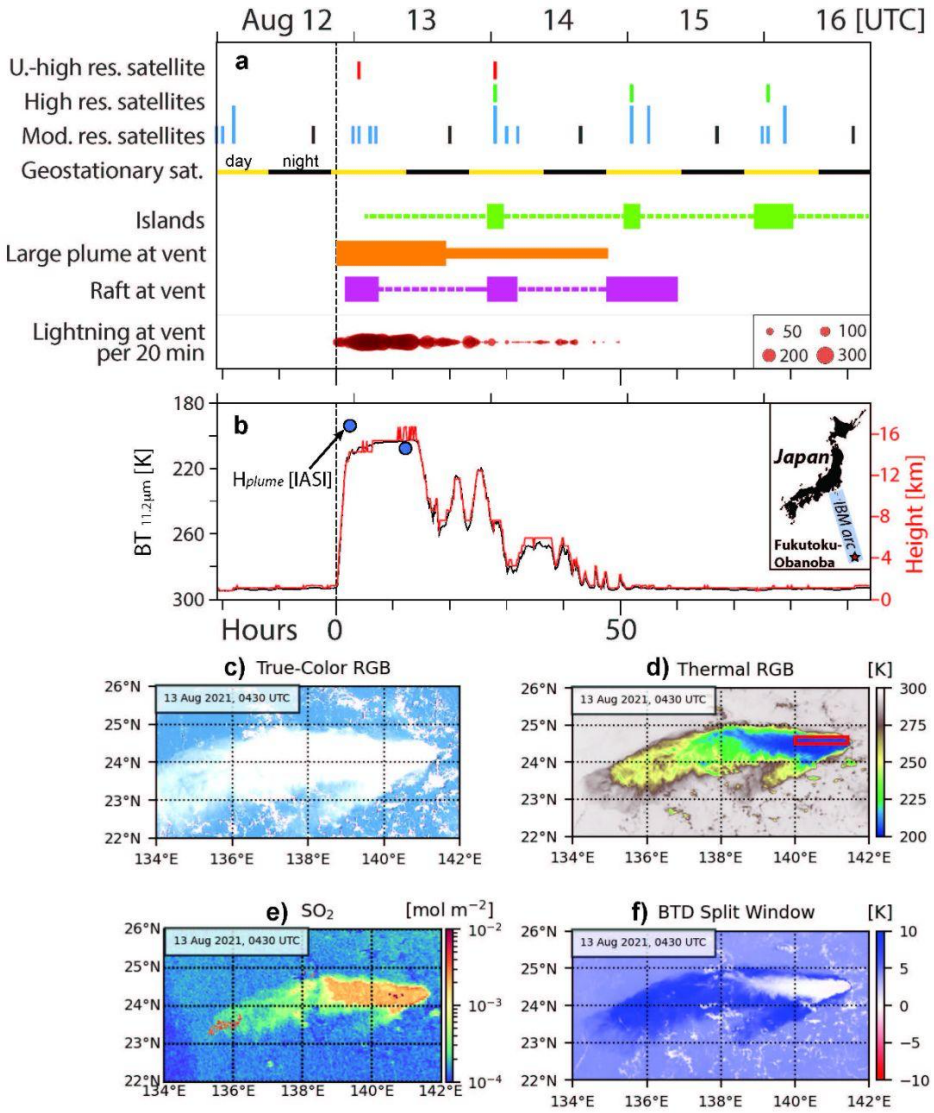

Figure 1: August 2021 eruption timeline. a) Summary of satellite availability and observations of eruption features. b) Plume height through time calculated from Himawari-8 brightness temperature and compared to Infrared Atmospheric Sounding Interferometer (IASI) data. c) True color image of the volcanic plume at 4:30 UTC on August 13, 2021. d) 11.2 μm brightness temperature of the volcanic plume. The red box shows the domain over which plume height was measured in panel **b**. e) SO_2 measurements within the plume. f) The 11.2-12.4 μm brightness temperature difference of the plume.

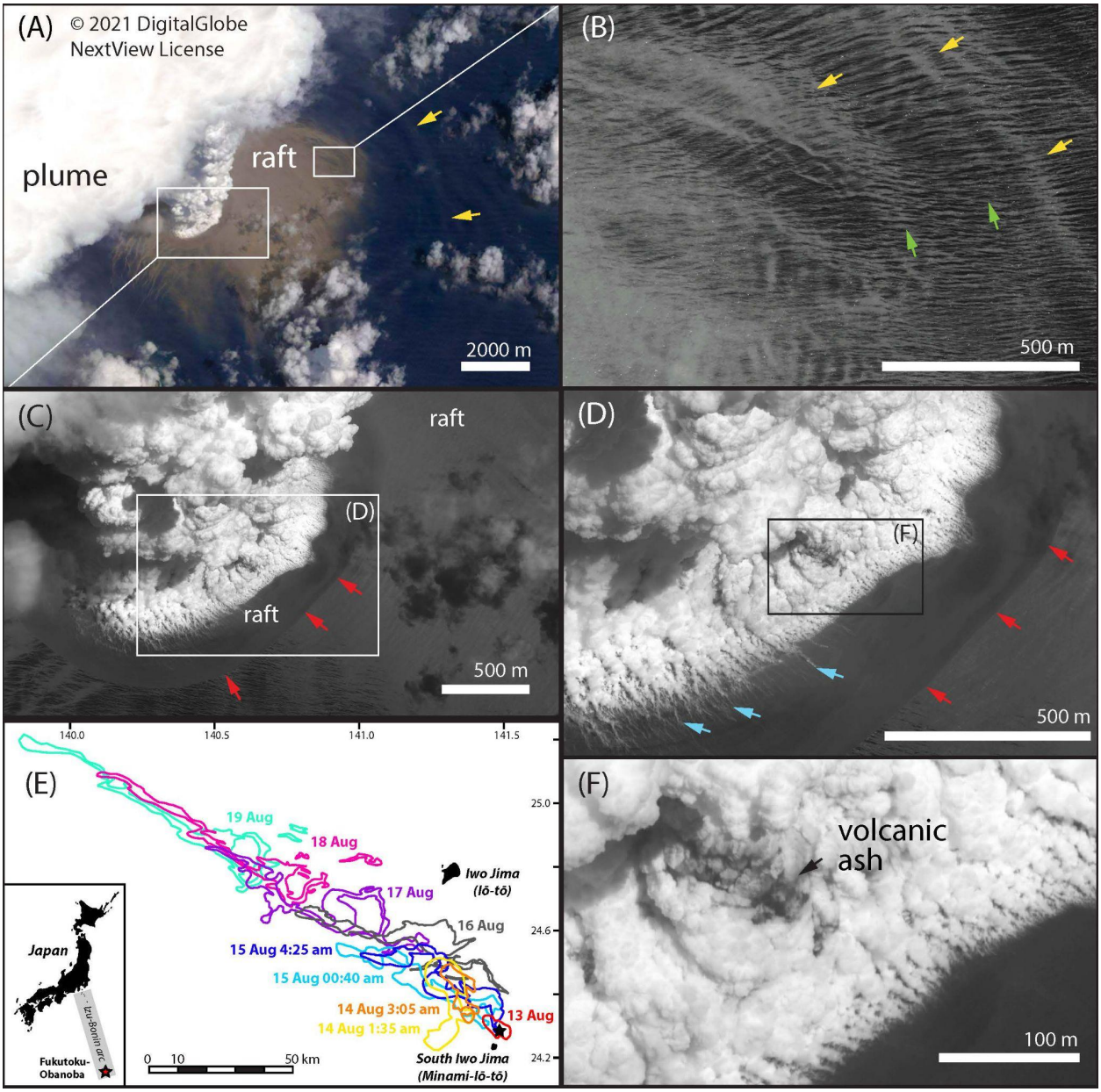

Figure 2: All images except (E) are (c)2021, DigitalGlobe, Inc., a Maxar company; NextView License and show the aerial plume and/or pumice raft on 2021/08/13 01:22 UTC (four hours

after eruption onset). (A) A bright white aerial plume and a pumice raft that has spread up to 5 km from the vent. Radial blast waves are present (yellow arrows). (B) Fine-scale laminations within the August 13 raft (grey) are present and parallel to radial blast waves (yellow arrows) and ocean swell (green arrows). (C) Red arrows show the sharp contrast between new raft material and a slightly older and more dilute raft. (D) The contact between the white aerial plume and pumice raft. Contrails on the raft pointing towards the plume indicate cooling bombs (blue arrows). (E) Outlines of the raft over the first week of the eruption and extracted from multiple satellite sources. Raft is to the northwest. (F) A single ~100 m dark, and thus ash rich, region within the bright white plume.

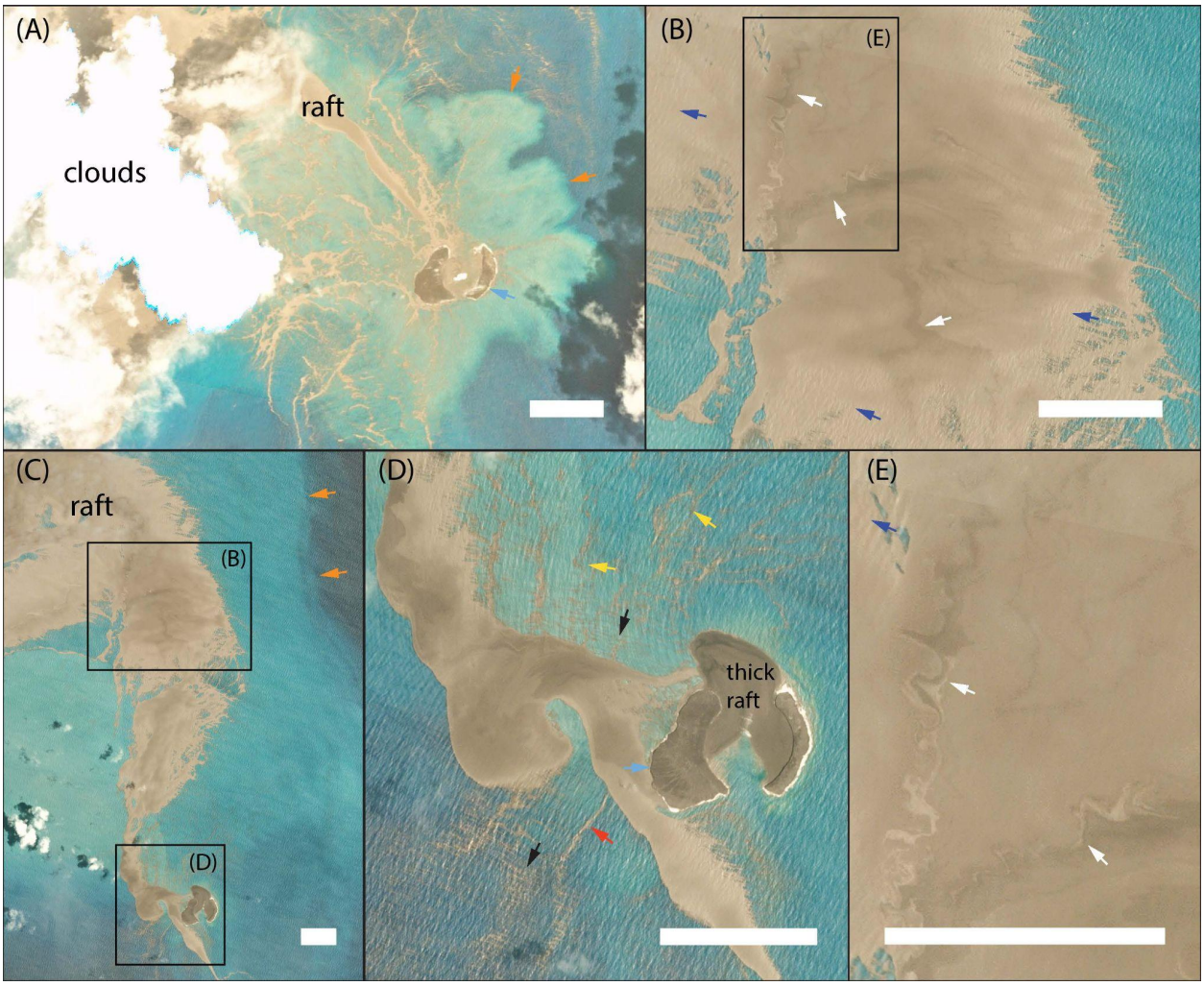

Figures 3: All imagery from Planet[55] and white scale bars are 1 km. (A) The raft and vent approximately 27 hours after eruption onset (2021/08/14 0:50 UTC). The two crescentic islands are present (blue arrows) and discolored water (orange arrows) can be distinguished from the raft. (B) A portion of the raft on 2021/08/15 0:50 UTC. The ocean swell is visible within the lightest (and thinnest) sections of the raft (blue arrows). Ribbon-like patterns are present within

the raft (white arrows) and may be caused by inter-raft collisions. (C) The raft and islands on 2021/08/15. Note the edge of discolored water (orange arrows). (D) Raft material leaving the vent area on 2021/08/15. Dark and thick raft exits from the northern gap between the two islands. White vapor at the crater center shows that wind direction is to the NW. Fragments of the raft are oriented parallel to the wind direction (black arrows), ocean wave direction (red arrows), and radial wave direction (yellow arrows). (E) Variations in color and thickness are present within the raft as are complex curves and swirls (white arrows).

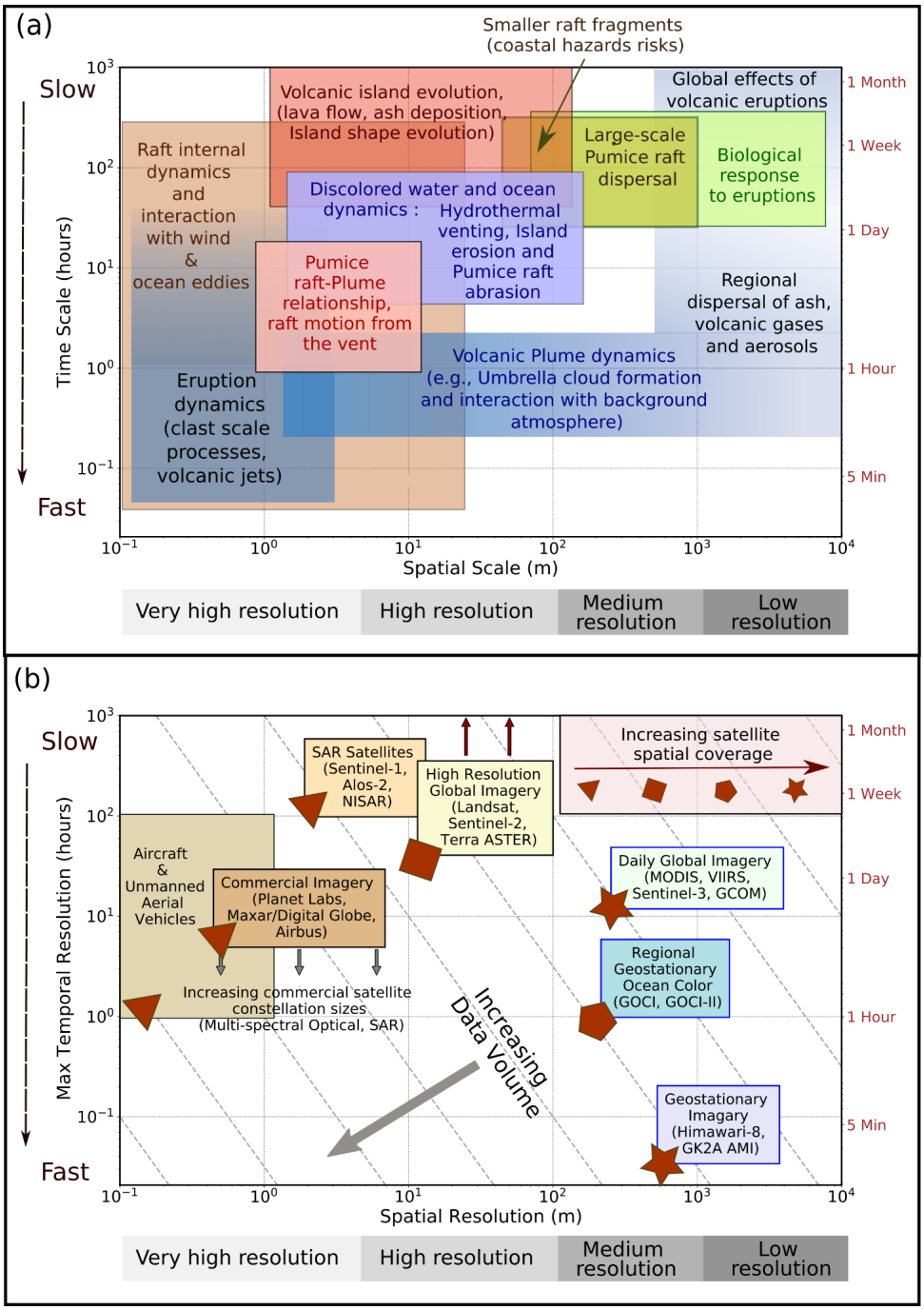

Figure 4: (A) Estimates of relevant timescales and spatial scales for important processes related to submarine volcanism. (B) Temporal and spatial resolutions of satellite data that can be used to examine volcanic processes. Data volume as plotted is estimated as proportional to 1/(resolution^2 x revisit time). That is, data volume as estimated is not dependent here on global coverage area or the spectral resolution/number of bands.

Supplementary Materials for

Simultaneous creation of a large vapor plume and pumice raft by a shallow submarine eruption

Kristen E. Fauria[1*], Martin Jutzeler[2], Tushar Mittal[3], Ashok Gupta[1], Liam J. Kelly[1], John Rausch[1], Ralf Bennartz[1], Brent Delbridge[4], Lise Retailleau[5,6]

Correspondence to: kristen.fauria@vanderbilt.edu

This PDF file includes:

Other Supplementary Materials for this manuscript include the following:

Materials and Methods

Initial volume flux

To determine the initial plume volume flux we assess the area of the plume top in the first 110 minutes of the eruption. During this initial time period the plume expands as a steady intrusive density current at its level of neutral buoyancy. We fit a model of plume top radius as a function of time to solve for flux, $r = (\frac{3\lambda Q N}{2\pi})^{1/3} t^{2/3}$, where λ is a constant that is approximately 0.2, Q is the volume flux, N is the brunt-vaisala frequency that describes the ambient stratification, and t is time[23]. To estimate the plume top area we use Himawari-8 brightness temperature data at 11.2 microns. Our visual analysis showed that most plume tops were between 190 and 210 K and thus we chose 210 K as a threshold for calculating initial plume top area. Because the plume top was elongated in the western direction due to wind, we calculated the circular equivalent radius of the plume top, $r = \sqrt{\frac{A}{\pi}}$, where A is the measured plume top area. Using an estimate of $N = 0.02$ s^{-1} from ERA5 reanalysis data, we fit this power-scaling to our measurements of spherical-equivalent plume top radius through time. We find that the $t^{2/3}$ scaling fits the data well for the first 110 minutes and determine an initial flux Q = 1.5x10^9 m^3 s^{-1} [Fig. S1].

Plume height

We used the Himawari-8 channel at the wavelength of 11.2 microns to estimate plume height through time. For this calculation we considered mean 11.2 microns brightness temperature (BT) values within the rectangular box in Figure 1c (140-141.4°E and 24.3-24.5°N). This domain captured the plume well during the first 12 hours of the eruption, however as the plume became smaller and unsteady it did not always fill the entire averaging box. Clouds passing overhead cause meteorological contamination of the brightness temperature data and we note that there is minor meteorological contamination within the plume height data on August 14. We manually replaced the meteorological cloud BT value with clear-sky BT values starting on August 15 when we visually confirmed a lack of new volcanic activity in the Himawari-8 data. After acquiring BT values, we converted these values to plume height using ERA5[56], which provides reanalysis data for atmospheric temperature profiles. To verify our plume height estimates, we compared against SO_2 plume height data from Infrared Atmospheric Sounding Interferometer (IASI)-Metop C [blue dots in Fig. 1b], total attenuated backscatter profile at 532 nm from space-borne lidar (CALIPSO, Fig. S7), and profile of aerosol-to-molecular extinction ratio from Stratospheric Aerosol and Gas Experiment (SAGE) III on ISS[57] for the available overpass. We find close agreement between the estimates, including on 2021/13/08 at 17:40 UTC from IASI-Metop C. We note that plume height values of ~1.5 km in Fig. 1b are not significant and are equivalent to estimates of plume height on clear-sky days.

Background Atmospheric Conditions

We determined the mean tropopause height where the temperature decreases with height at a rate of no more than 2 K km^{-1} [58]. We used hourly ERA5 data to estimate the mean tropopause height during 12-18 August 2021 based on the above definition. Over Fukutoku-Okanoba (24.28°N, 141.48°E), the mean tropopause height during 12-18 August 2021 is found to be 15.5 +/- 0.5 km.

We also used hourly ERA5 reanalysis data to calculate the Brunt Väisälä frequency for the same period covering 12 to 18 August 2021. Brunt Väisälä frequency describes the frequency at which an air parcel oscillates in a stably stratified atmosphere

$$N^2 = \frac{g}{\theta}\frac{d\theta}{dz},$$

where θ [K] is the potential temperature, g [m s^{-2}] is gravitational acceleration, and z [m] is the height. Over Fukutoku-Okanoba (24.28°N, 141.48°E), the estimated mean value of Brunt Väisälä frequency (N) near tropopause height is 0.02 s^{-1}.

Plume composition

The sign and magnitude of brightness temperature difference between thermal infrared bands at 11.2 and 12.4 μm (hereafter, $BTD_{11.2-12.4\mu m}$) allows for the identification of liquid water, ice, or ash within the plume (e.g., Legrand et al., 2001). On 13 Aug 2021 at 0430 UTC, the positive value (blue color in Fig. 1e) of $BTD_{11.2-12.4\mu m}$ indicates thin ice clouds, whereas the negative value (red color near the vent in Fig. S8) represents ash. Near zero value of $BTD_{11.2-12.4\mu m}$ (white color in Fig. 1e) at brightness temperatures below roughly 230 K depict thick ice clouds [Fig. 1]. Overall, the sign and magnitude of $BTD_{11.2-12.4\mu m}$ for this eruption shows that it is ice-rich.

Lightning

Approximately 10,500 lightning flashes were reported by the World Wide Lightning Location Network (WWLLN) within 40 km of Fukutoku-Okanoba between eruption onset and 2021/08/15. On average, 200-300 flashes/20 minutes were observed during the first day of the eruption and the timing of these high lightning flash rates correlates well with the initial stratospheric phase of plume activity [Fig 1].

Erupted Volume Calculations

We calculated the raft volume following the methods outlined by[7,8] and by using estimates of raft area from satellite images on August 14 - 16. We estimate an average area of the early raft of 250 km^2. This calculation does not include very thin rafts that are not well detected by reflectance methods, and may increase the affected area by ca. 50 km^2. We use in situ observations of past rafts and a calibration between raft thickness and ocean swell damping[8] to estimate an average raft thickness of 40 cm. By multiplying the raft area by an average thickness of ca. 40 cm, the raft volume is about 100 mio m^3. Considering a packing of clasts at 60%, we estimate a pumice volume of 60 mio m^3. Based on an average pumice vesicularity of 70%,

which is conservative for intermediate pumiceous compositions (Jutzeler et al. 2019), the dense rock equivalent (DRE) volume is 18 mio m^3.

The newly formed islands were initially made of two partially submerged crescentic tuff rings (400 and 200 m in width, and 870 and 800 m in length, respectively). We estimate an average island elevation of 15 m based on Japan Coast Guard images and later confirmed by[59] [Figs. S8-S9]. Together these dimensions give a total subaerial volume of ca. 6 mio m^3.

We use pre-eruption bathymetry to estimate the volume of the new underwater deposits. In 2010 Fukutoku-Okanoba was a flat top, conical volcano (ca. 1.2 x 1.7 km) that was 29-40 m below sea level. Because the total combined diameter of the two crescentic islands (1.1 km) was similar to the pre-eruption area of the volcanic summit, we conclude that the 2021 eruption products covered most of the 2010 summit. We use a truncated cone geometry to estimate a minimum volume $47x10^6$ m^3 (1.2 km x 1.7 km base, 1.1 km x 1.1 km top, and 40 m thickness). This volume calculation does not include the unknown volume of material that was sedimented downslope of the volcano. Further, the volume of the products from the small 2010-2021 eruptions are unaccounted for, however are likely minimal.

Supplementary Text

Seismicity Observations

Seismicity often occurs along with or before volcanic activity. For this reason, it is one of the means used to monitor the activity of many volcanoes. However, in isolated areas with little risk for the population data is often lacking. JCJ (JP network) was the closest station from the eruption from which seismic recordings were available at the time of the eruption (Fig. S2). Station JCJ is located more than 300 km away from the eruption. Consequently, the station likely would not be able to record small seismicity from the eruption.

We represent the signals recorded on the vertical component of station JCJ the day before and after the start of the eruption (12th and 13th August, 2021, available through the IRIS data center). Nothing clear can be observed on the signals until 2021/08/12 21:00 UTC when signals propagated from a sequence of teleseismic earthquakes (highlighted by the blue rectangle on Fig. S3) from the South Sandwich islands region were recorded by the station (with a M 8.1 strongest earthquake at 2021/08/12 18:35 UTC).

After the beginning of the eruption, some seismicity can be observed. Early on the 13th, two signals were recorded that could be linked to the eruption (green rectangle on Fig. S3). Moreover, a magnitude 4.1 earthquake was cataloged by the USGS on the 14th, very close to the eruption (orange dot on Fig. S3).

SO_2 Tropomi Data

On August 12, 2021, there was no visible ash/SO_2 plume for many of the instruments (TROPOMI, AIRS, OMPS, OMI) with data available during the eruption at Fukutoku-Okanoba. IASI-Metop A and B and GOME-2 visible SO_2 vertical column on August 12, 2021, however these were 12-12:30 AM UTC, before the eruption had begun. All instruments except IASI-Metop A, IASI-Metop B, and AIRS at night showed SO_2 vertical column data on August 13, 2021. Areas of SO_2 span around 1 degree in longitude west of Fukutoku-Okanoba. Values for vertical column are mostly between 2 and 5 DU, with maximums reaching 10-20 DU. SO_2 plume heights at the vent source are around 10 km, with distal heights reaching 18 km. On August 14, there is still SO_2 vertical column data around the same area, but it is more spread out than August 13, both decreasing in latitude expanse and increasing in longitude expanse. Highest values are now between 5-10 DU. SO_2 plume heights are similar to August 13, with the closest measurements to the vent being 8-10 km and the highest still reaching up to 18 km further from the volcano, see by IASI-Metop A/B. By August 15, the concentrated SO_2 signature had mostly dissipated. There were some areas where SO_2 was present, but values are between 1-2 DU, a marked decrease from the previous days.

Other eruption associated products

Discolored water is a pervasive feature that is present in most raft and eruption imagery [e.g., Fig. 3] We identified three distinct sources of discolored water: 1) discolored water sourced from the vent; 2) discolored water closely following the raft; 3) discolored water due to erosion of the island. Discolored water at the vent was likely generated directly from the eruption, hydrothermal fluids, or erosion of the new island. Discolored water proximal to the raft likely corresponds to intense abrasion of the pumice clasts, and is visible because floating pumice and sinking products of pumice abrasion are dispersed differently depending on their depth in the water column (Jutzeler et al. 2014, 2017, 2020).

Satellite images show that the eastern and western crescentic islands were eroded below sea level by early November 2021 and late December 2021, respectively [9]. Although we focus on the dynamics of the raft generated directly from the 2021 eruption, tiny dilute rafts and areas of discolored water were formed from island erosion and mass-wasting for weeks after the eruption.

Space-Borne Lidar (CALIPSO)

We utilize the Cloud-Aerosol Lidar with Orthogonal Polarization (CALIOP) onboard CALIPSO [60] overpass near Fukutoku-Okonoba on 2021/8/13 at 17:40 UTC to compare plume height estimated from Himawari-8 and ERA5 data. The CALIPSO's total attenuated backscatter coefficient provides information on the vertical structures of clouds and aerosols [60]. Fig. S7 shows the time-height cross-section of CALIPSO's total attenuated backscatter coefficient (km^{-1} sr^{-1}) at 532 nm near the submarine eruption site. The total backscatter lidar signal shows that aerosol loads and cirrus layers extend the height range between 14.5 and 16.5 km, which agrees

with the plume height estimated for the corresponding overpass from Himawari-8 *(Figure not shown)*.

Spectral signatures

To examine the spectral characteristics of water and pumice rafts surrounding Fukutoku-Okanoba, we used data from the OLCI instrument aboard Sentinel-3 to generate RGB images of three time periods during the eruption and using ESA's Sentinel Application Platform (SNAP). We selected areas of interest for spectral information by placing pins in representative areas of the pumice raft, different areas of discolored water, and regular ocean water. Spectral information (reflectance) for all bands was collected and plotted against band wavelengths. 3 days were chosen for study: 2021/8/14, 2021/8/16, and 2021/8/20. They show the pumice raft at different locations respective to the vent. On 2021/8/14, the raft was close to the subaerial plume and eruptive vent. By 2021/8/16, it had moved west and elongated, and by 2021/8/20 it was even further west and dispersed into multiple individual segments.

The graph showing reflectance on 2021/8/14 shows different areas of pumice rafts having similar shapes to their reflectance curves [Fig. S10]. The discolored water signals do not show clear similarities. This is possibly due to the presence of the ash plume causing noise in the image.

In the next 2 charts [Figs. S11-S12], the differences between the pumice raft, light blue discolored water around the pumice raft, greenish discolored water around Iwo Jima and the vent, and regular ocean water. Different pins on the pumice raft show this parabolic curve that peaks between 700 and 800 nm. Light discolored water around the pumice raft shows a peak between 450-500 nm with a steep decline afterwards. Green discolored water signatures around Iwo Jima and the vent show spectral peaks closer to 500 nm and before 600 nm but also show a decline that is more shallow. Ocean water peaks at 400 nm and steeply declines afterwards. Spectral signatures of discolored water around the pumice raft and discolored water around Iwo Jima and the vent are distinctly different.

Figures S1 to S13

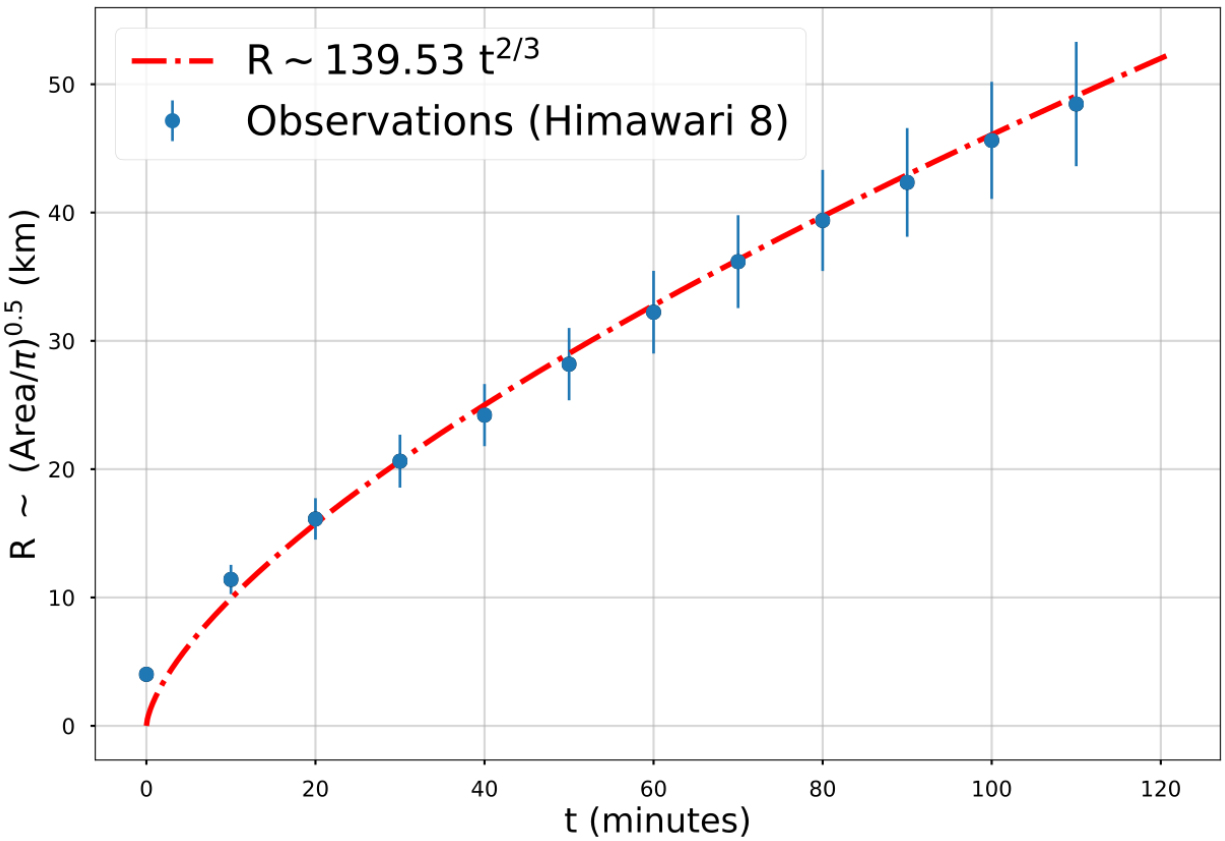

Fig. S1.

Fit between time and plume top area. Radius scales with time (in seconds) to the ⅔ power ($R \sim 139.52t^{2/3}$).

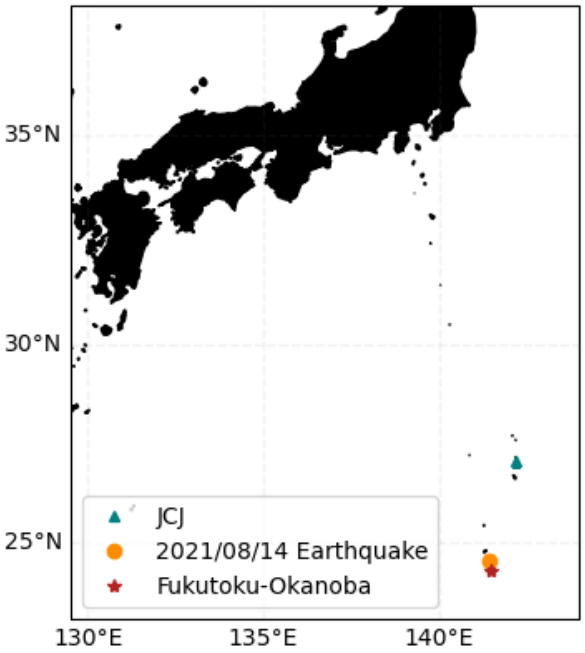

Figure S2.

Map of the eruption location (red star), seismic station (teal triangle) and a close earthquake.

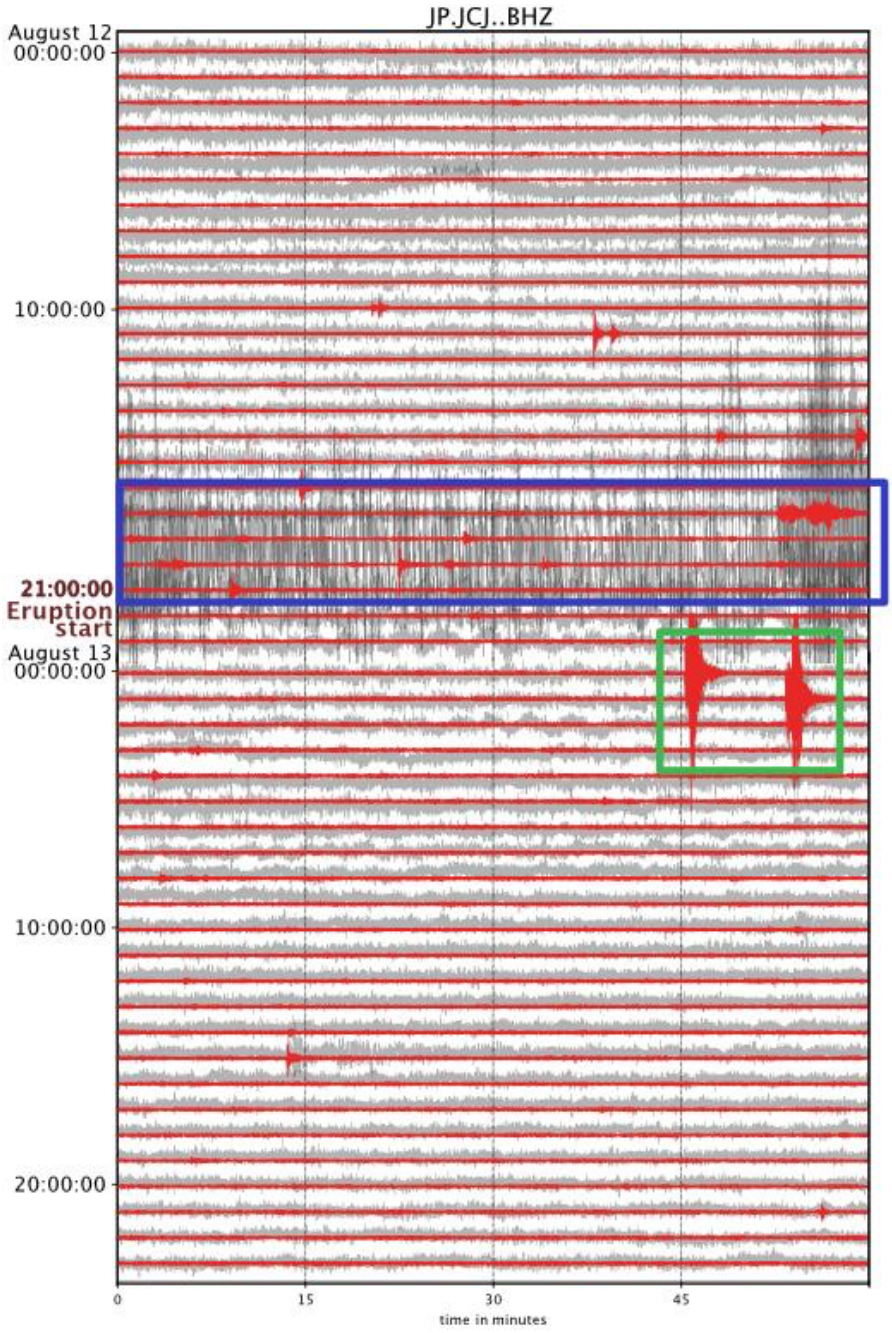

Fig. S3.

Vertical component of the signals recorded by station JCJ, Chichijima Island on 12th and 13th October, 2021. The grey timeseries represent the raw signals and the red timeseries represent the signal with a high pass filter at 1 Hz. The blue rectangle highlights signals generated by teleseismic earthquakes. The eruption start is highlighted (at ~ 21:00 - 21:10 UTC, Dec 12th) . The green rectangle represents two strong events that could be linked to the eruption.

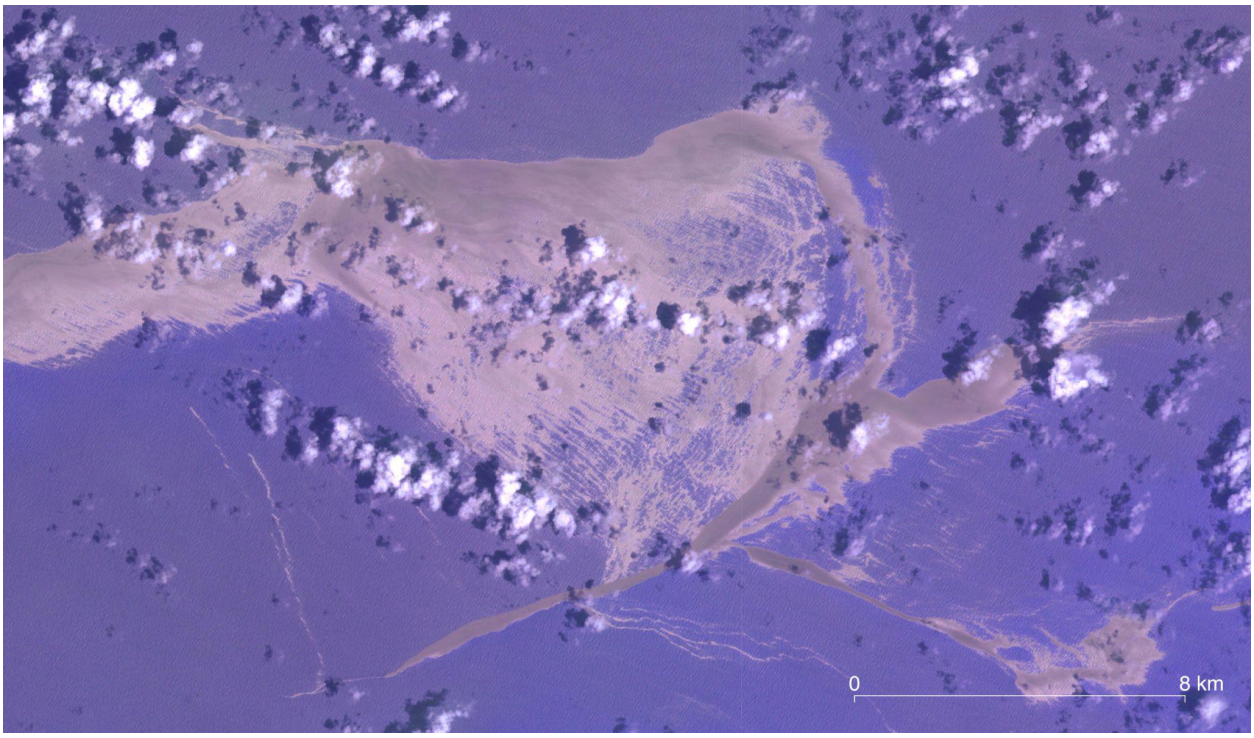

Fig. S4.

This ASTER image of the Fukutoku-Okanoba raft from 1:20 UTC on August 16 shows the characteristic checkerboard pattern of interacting dispersal from ocean waves and wind. There are also differences in raft color that are indicative of variations in raft thickness.

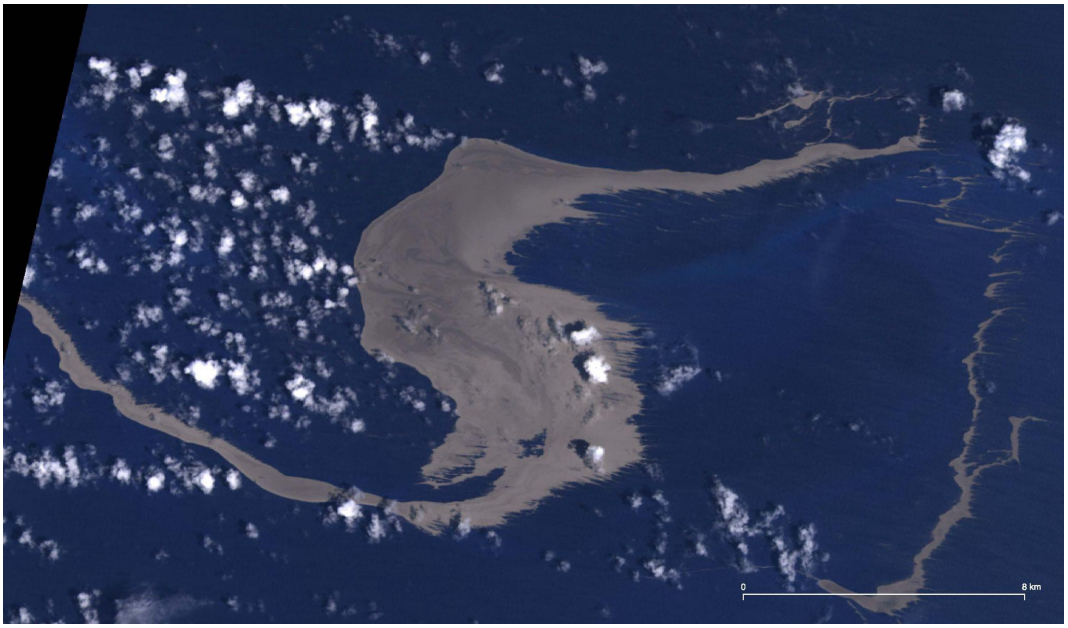

Fig. S5.

The Fukutoku-Okanoba raft on August 17 at 1:00 UTC and from Landsat8. Complex structures are visible within the raft. We interpret the variations in color to be representative of variations in thickness.

Fig. S6. Japan Coast Guard image of an eruption at Fukutoku-Okanoba on December 1, 1986. Note the white vapor plume, jets of volcanic particles, and pumice raft on the sea surface.

827
828

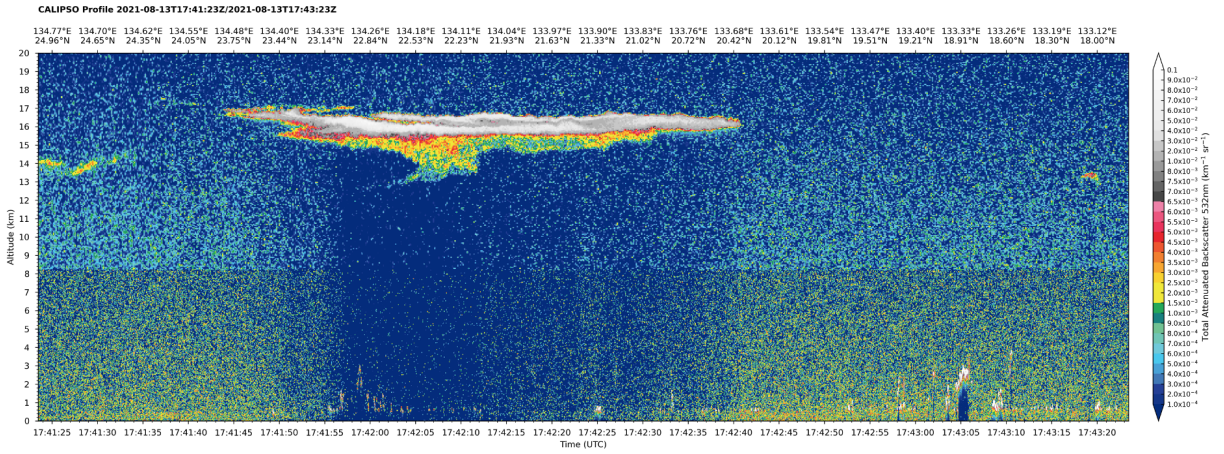

829
830 **Fig. S7.** A profile of CALIPSO space-born LiDAR data on 8/13/2021 at 17:40 UTC shows the
831 Fukutoku Plume height to be ~16.5 km, consistent with plume height estimates from Himawari-
832 8.

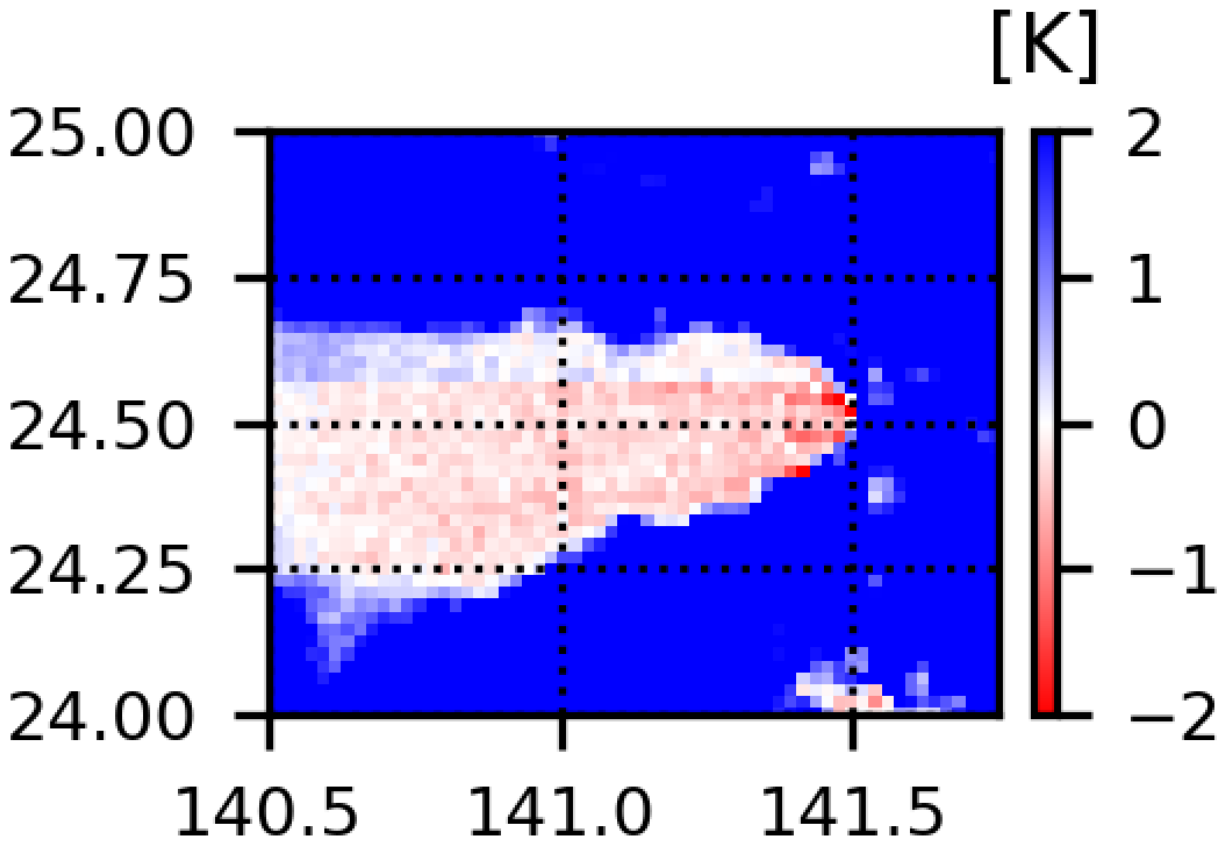

Figure S8.

Brightness temperature difference ($BTD_{11.2-12.4\mu m}$) of the Fukutoku-Okanoba ash plume on 13 Aug 2021 at 0430 UTC. The x-axis is in longitude and the y-axis is latitude. The slightly negative BTDs near the vent could indicate the presence of volcanic ash in the plume.

Fig. S9.
Japan Coast Guard image (2021/8/26 13:07 local time) of the new island created by the 2021 Fukutoku-Okanoba eruption. The eastern island is almost fully eroded by this time. Discolored water is emanating from the island as well. Image credit: Japan Coast Guard 3rd Regional Coast Guard Headquarters.

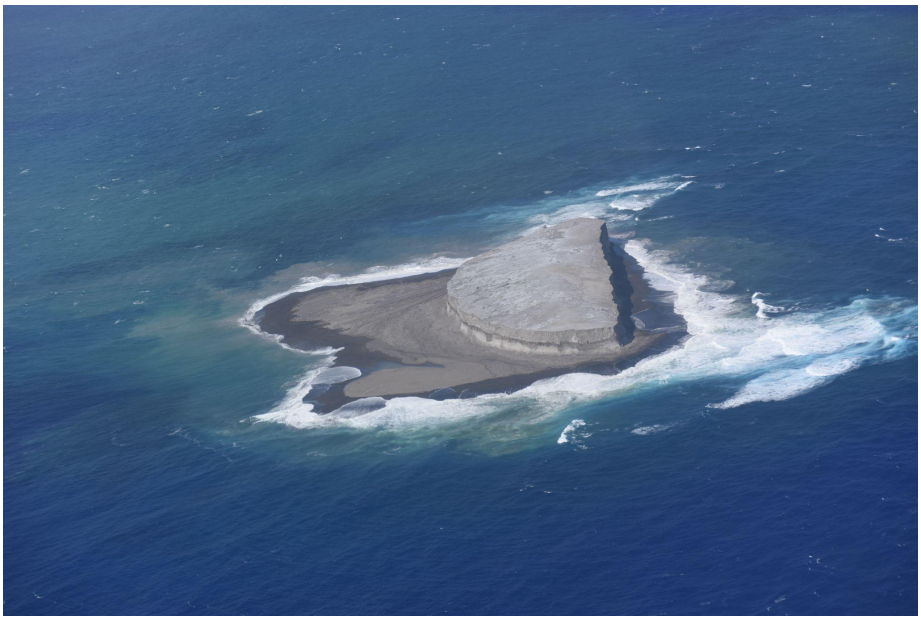

Fig. S10.

Japan Coast Guard image (2021/10/12 13:13 local time) of the Fukutoku-Okanoba island. Within this image we can see scattered metric-sized blocks amongst finer grained tephra. Further, the surface of the island has already developed drainage systems, and a terrace is formed on the western island, likely delineating the high-tide mark. Eastern Island has ca. 30 m cliffs and as confirmed by [59].

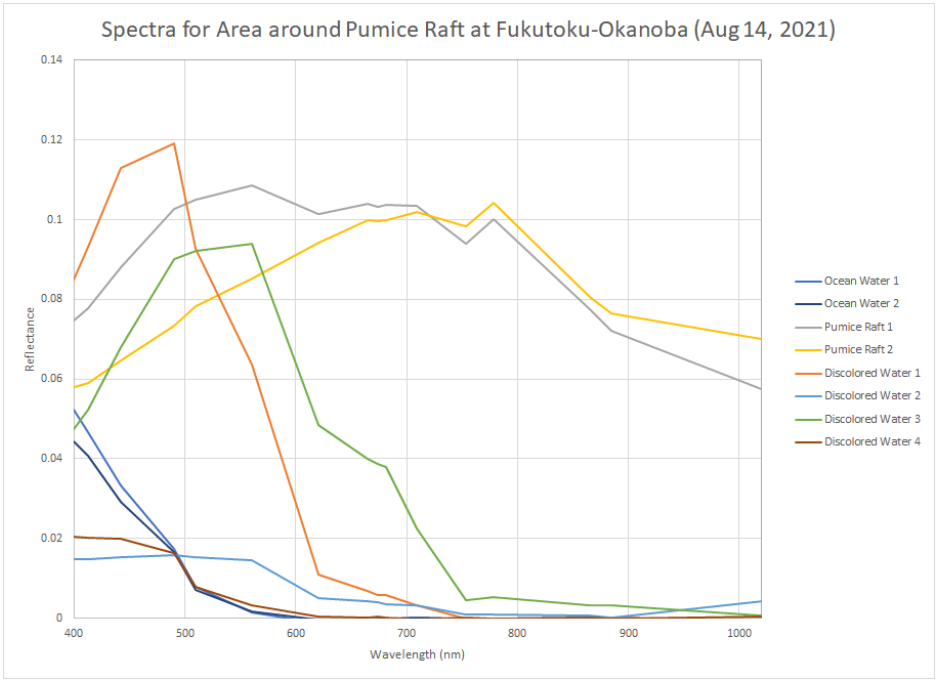

Fig. S11. Spectra of ocean water, pumice raft material, and discolored water around Fukutoku-Okanoba on August 14, 2021. These data are from the OLCI instrument aboard Sentinel-3 and show that ocean water, discolored water, and pumice rafts have different spectral signatures.

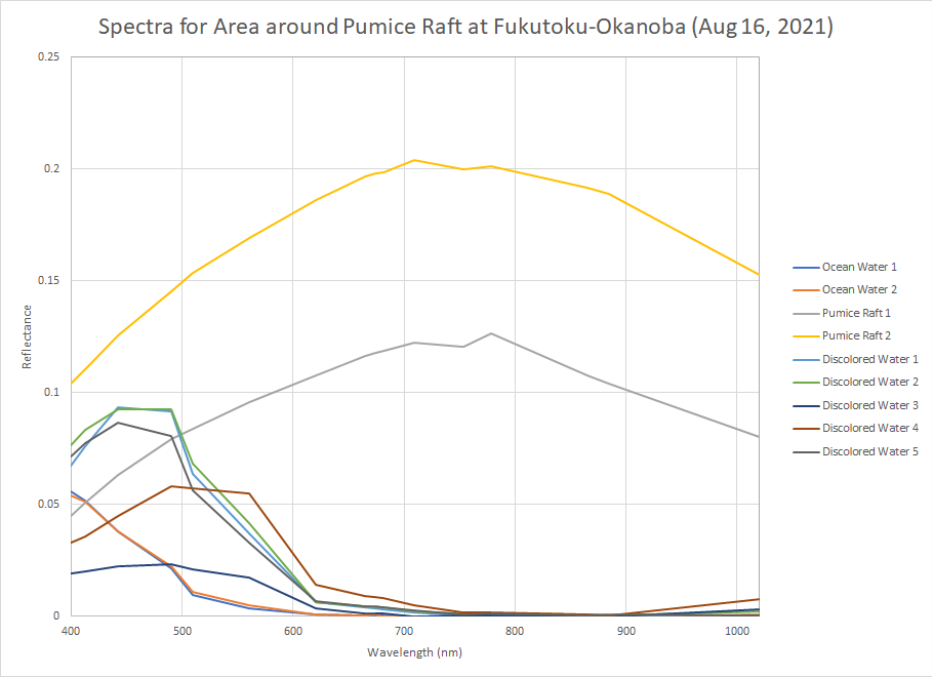

Fig. S12. Spectra of ocean water, pumice raft material, and discolored water around Fukutoku-Okanoba on August 16, 2021. These data are from the OLCI instrument aboard Sentinel-3 and show that ocean water, discolored water, and pumice rafts have different spectral signatures.

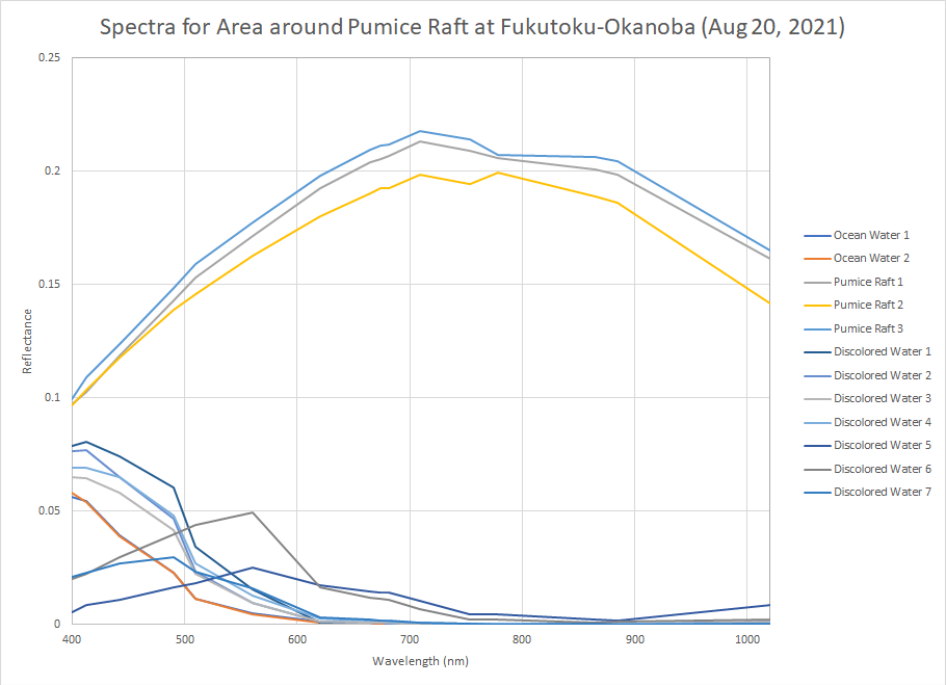

Fig. S13. Spectra of ocean water, pumice raft material, and discolored water around Fukutoku-Okanoba on August 20, 2021. These data are from the OLCI instrument aboard Sentinel-3 and show that ocean water, discolored water, and pumice rafts have different spectral signatures.

Fig. S14.
Japan Coast Guard Image of the August 2021 Fukutoku-Okanoba eruption column. Note the spread of the neutrally buoyant umbrella cloud. This image was taken from an altitude of ~6,000 m and from 90 km north of Fukutoku-Okanoba on 2021/8/13 between 15:00 and 15:30 local time. Image credit: Japan Coast Guard 3rd Regional Coast Guard Headquarters.

Table S1

Summary of satellite imagery that was available for visual analysis of the Fukutoku-Okanoba raft or vent area by this study.

	Timestamp (UTC)										
Date	SENTINEL3	TERRA	AQUA	SUOMI	ASTER	Landsat8	PLANET-a	PLANET-b	PLANET-c	DigitalGlobe	SUOMI night
2021-08-12	0:40	1:45	3:20	3:40							17:00
2021-08-13	0:15	0:50	4:05	3:20						1:22	16:40
2021-08-14	0:50	1:35	4:45	3:05			0:50				16:20
2021-08-15	1:00	0:40	3:50	4:25			0:50	1:40			16:00
2021-08-16	0:35	1:20	4:35	4:05	1:20						15:45
2021-08-17		2:05	3:45	3:50		1:00	1:10				
2021-08-18	0:45	1:10	4:20	3:30			0:25	0:49	21:55		
2021-08-19	1:00	1:50	3:25	3:10							
2021-08-20	0:30	0:55	4:10	2:50							
2021-08-21	1:10	1:40	3:15	4:20			21:55				
2021-08-22	0:40	0:45	3:55	3:55							
2021-08-23	0:55	1:25	4:40	3:35							
2021-08-24	0:30	2:10	3:45	3:15							

Movie S1

Brightness temperature (BT) over the Fukutoku-Okanoba area from August 12 - 17, 2021 and assessed using Himawari-8. Fukutoku-Okanoba is located at the red dot and the data is shown in 10 minute intervals. The volcanic plume can be seen in the BT data and is observable at night.

Movie S2

Visual imagery (true color RGB) from Himawari-8 and of the Fukutoku-Okanoba area from August 12 - 17, 2021. No imagery is available at night. The plume is bright white and the pumice raft can sometimes be seen in tan. The location of Fukutoku-Okanoba is shown with a yellow pin.